IJME

Int. J. of Applied Mechanics and Engineering, 2026, vol.31, No.2, pp.140-154
DOI: 10.59441/ijame/218549

FLOW OF Cu-Al2O3/WATER NANOFLUID PAST A TIME-DEPENDENT RADIALLY STRETCHING SHEET

M.V. Sreekantha Reddy[1] and D. Srinivasacharya[2*]
[1]Mathematics, Gokaraju Rangaraju Institute of Engineering and Technology, Hyderabad, INDIA
[2]Mathematics, National Institute of Technology, Telangana, INDIA
E-mail: dsc@nitw.ac.in

The steady laminar flow past a time-dependent radially stretching sheet within a hybrid nanofluid is studied. The governing equations are converted into ordinary differential equations utilizing the similarity transformations. Successive linearization is applied to linearize the nonlinear system of equations. The resultant system of equations is solved using the Chebyshev collocation method. Plots demonstrating velocity, temperature, Nusselt number, and skin friction coefficient for a few chosen parameters are shown. When volume fractions of Cu-containing nanoparticles rise, the critical values of these parameters fall, and when alumina (Al_2O_3) nanoparticle volume fractions rise, they increase. Compared with the nanofluid on the radially stretched surface, the hybrid nanofluid transfers heat faster. The addition of more alumina nanoparticles also lowers the Nusselt number and raises the skin friction coefficient. Furthermore, adding more copper (Cu) nanoparticles lowers the skin friction coefficient and the local Nusselt number on the stretching surface. This study is important because it demonstrates how hybrid nanofluids can be engineered to optimize heat transfer and flow resistance over stretching surfaces, providing valuable guidance for improving thermal performance in industrial and engineering applications.

Key words: Nusselt number, hybrid nanofluid, radially stretching sheet, successive linearization, skin friction coefficient.

1. Introduction

The analysis of fluid motion across radially stretched sheets is essential due to its significance in metallurgy, chemical and biomedical engineering, metal spinning, hot rolling, polymer extrusion, and liquid metal. This flow is particularly important in balloon expansion, aerodynamics, plastic film drawing, and other fields. The flow induced by an unsteady stretched sheet is one type of flow problem relevant to polymer extrusion. The end product is contingent upon the stretching rate and the cooling rate; thus, the selection of cooling liquid is crucial as it directly influences both the stretching rate and the cooling rate. Otherwise, abrupt stretching may disrupt the characteristics of the final product. Numerous researchers have examined the features of mass and heat transmission both in several types of fluid flows. Khan *et al.* [1] addressed the heat transfer and axially symmetric motion of a cross fluid on a sheet that is stretched radially. Ahmed *et al.* [2] investigated how radiation and an angled magnetic field affected the Sisko fluid's pass across a sheet that is stretched radially. Sreelakshmi *et al.* [3] explored the time-dependent Jeffrey nanofluid flow across a surface that is expanding radially by employing convective boundary conditions. An extended sheet involving several slips, radiation, chemical reactions, and magnetic impacts was the subject of an investigation by Khan *et al.* [4]. The consequence of a chemical reaction on the transfer of mass across a radially stretched sheet has been investigated by Nayak *et al.* [5]. Most research on the radially expanded surface focuses on steady-state conditions. On the other hand, unsteadiness becomes a crucial subject of analysis in many engineering processes. The influence of axially symmetrical motion and heat transfer on a surface that is stretched with time out in a radial direction has been examined by Shahzad *et al.* [6-7]. Srinivasacharya and Shravan Kumar

* To whom correspondence should be addressed

[8] used artificial neural networks to investigate the movement of Casson fluid across an unsteady sheet that is expanding radially under the influence of Soret and Dufour.

The topic of heat transfer enhancement has garnered a lot of attention in the last several years. Since nanoparticles have a higher thermal conductivity than base fluid, thermal scientists have proposed including metallic or non-metallic nanoparticles in the base fluid to boost its thermal conductivity. A nanofluid is the resultant blend with enhanced chemical and physical characteristics. In the year 1995, Choi and Eastman [9] coined the term "nanofluid". While nanofluids have demonstrated substantial improvements in heat transfer efficiency, their widespread adoption has been hindered by challenges such as particle aggregation, sedimentation, and limited stability. To overcome these limitations, researchers have turned to hybrid nanofluids to enhance heat transfer capabilities. Hybrid nanofluids combining two or more types of nanoparticles or by adding other component to the nanofluid system, aiming to optimize the overall thermal performance. By integrating various nanoparticles, such as metal oxides, carbon-based materials, or organic compounds, HNFs exhibit superior properties, including enhanced thermal conductivity, improved stability, and increased adaptability, distinguishing them from traditional nanofluids. Hybrid nanofluids have applications in heat transfer within microelectronics, microfluidics, manufacturing, and medicine. Hybrid nanofluid provides better thermophysical qualities, thereby enhancing heat transfer efficiency. Hybrid nanofluids find extensive applications across multiple domains, including electronic cooling systems, automotive radiators, heat pipes, heat exchangers, as well as coolants used in welding and machining processes, and in nuclear facilities, among others.

In recent years, researchers have extensively studied how hybrid nanofluids transfer heat in boundary layer flows. Devi and Devi *et al.* [10-11] examined $Cu\text{-}Al_2O_3$ nanoparticles regardless of magnetic effects when studying the motion of a hybrid nanofluid across a stretched surface. They discovered that, compared to ordinary nanofluid, hybrid nanofluid increases the heat transmission rate. Hayat *et al.* [12] analyzed the effects of chemical reactions, thermal radiation, and heat generation on the three-dimensional steady rotating flow of hybrid nanofluid along a stretched sheet. They found that the heat transmission rate of hybrid nanofluid is greater than that of simple nanofluid. Yousefi *et al.* [13] investigated analytically the steady-state three-dimensional stagnation-point flow of an aqueous titania-copper hybrid nanofluid around a circular cylinder that exhibits sinusoidal radius change. Subhani and Nadeem *et al.* [14] proposed a numerical solution for the flow of micropolar hybrid nanofluid over an exponentially stretching surface within a porous medium. Ghadikolaei *et al.* [15] examined the influence of an applied magnetic field on the stagnation-point flow of an electrically conducting hybrid TiO_2-Cu water nanofluid across a stretched sheet. Usman *et al.* [16] studied the flow of copper-alumina hybrid nanofluid over a permeable surface, considering nonlinear radiation and variable thermal conductivity. Rostami *et al.* [17] formulated two solutions for the mixed convective stagnation-point flow of a hybrid nanofluid composed of alumina and silica. Waini *et al.* [18,19] analyzed the unsteady hybrid nanofluid flow past a stretching/shrinking sheet and permeable stretching sheet with convective boundary conditions. Das *et al.* [22] studied computational analysis on MHD flow with water as base fluid and nanoparticles as aluminium oxide and copper induced by a convectively heated stretching sheet in presence of surface slip. Ali *et al.* [23] examined numerical thermal investigation of radiative magnetohydrodynamics axisymmetric $Cu\text{-}Al_2O_3/H_2O$ hybrid nanofluid flow over an unsteady radially stretched surface. Impact of variable fluid properties and viscous dissipation on hybrid nanofluid ($Cu\text{-}Al_2O_3/H_2O$) flow past a porous stretching sheet was explored by Abbas *et al.* [24].

The review of the current literature reveals a lack of discussion about the flow of hybrid nanofluid over radially shrinking and stretching sheets. Additionally, there are no published studies that examine the combined effects of unsteadiness and suction parameters on this fluid flow. Most of the studies on the radially stretched sheet are limited to steady-state scenarios. When flow is time-dependent, unsteadiness emerges as a critical factor in the analysis of various engineering processes. The behavior of hybrid nanofluids on a time-dependent radial stretching surface requires separate analysis because of the complex interactions and dynamics involved. The presence of various nanoparticles can greatly influence the flow behavior. The analysis of these interactions is crucial for enhancing the performance of hybrid nanofluids in a range of applications, including heat exchangers, cooling systems, and biomedicine. The separate analysis provides a deeper understanding of

the flow dynamics, which can lead to enhanced efficiency and effectiveness in these applications. Inspired by the unique advantages of hybrid nanofluids for thermal management and also to bridge the gap mentioned, this paper investigates the hybrid nanofluid flow and heat transmission across the time-dependent radially extending surface utilizing the Tiwari and Das [20] nanofluid model. Analyzing this flow is crucial for optimizing thermal management in dynamic industrial processes, as the stretching nature of a radial sheet significantly impact heat and mass transfer. Solving this model configuration mathematically can offer valuable insights for designing efficient cooling strategies in critical industrial processes, such as turbine blade cooling, chemical vapor deposition, and microelectronics fabrication. This can lead to improved performance, product quality, and significant energy savings. The novelty of the work is developing similarity solution for the flow past a time-dependent radially stretching sheet with constant temperature on the surface, using successive linearization to linearize the governing equations and then solving the resulting equations by the pseudo-spectral approach. The hybrid nanofluid is generated by scattering Alumina and copper nanoparticles in water. In the present problem the aluminum and copper nanoparticles are chosen because of their unique thermal properties. The combination of aluminum oxide and copper helps to maintain nanofluid consistency over time while also giving strong thermal characteristics. $Cu\text{-}Al_2O_3 : H_2O$ is one of the attractive choices for improved heat transfer in industries like electronics cooling, power generation and chemical processing. As copper is one the most thermally conductive metal enhances the thermal conductivity significantly and Al_2O_3 add stability and strength. The data of the current analysis is compared with the numerical results to verify the findings. $Cu\text{-}Al_2O_3$ hybrid nanofluids are more beneficial than single-particle nanofluids in industrial processes that require superior heat transfer enhancement and improved long-term stability in compact systems, which are achievable through the synergistic properties of the two different nanoparticles.

2. Materials and methods

2.1. Problem formulation

The unsteady and laminar flow of a hybrid nanofluid over a radially stretched surface is considered here. Figure 1 illustrates the coordinate system and geometry. In view of the rotational symmetry, all the physical quantities are independent of θ. Therefore, the azimuthal component of velocity vanishes. The surface is stretched symmetrically while maintaining the origin fixed by applying equal and opposite forces along the *r*-coordinates. Because of this configuration, the stretching can occur radially from the origin without changing its location. The flow is a consequence of the stretching of the radial surface, which has a time-dependent velocity $U_w = \frac{ar}{1-ct}$, which is linearly proportional to the distance *r* from the origin with a and c as positive constants having the dimensions of time^{-1}. The effective stretching rate $\frac{a}{1-ct}$ increases with time since $c > 0$. The temperature of the ambient medium is denoted by T_∞. Assume that the stretched surface is maintained at a temperature of the form $T_w = T_\infty + \frac{br}{1-ct}$, which represents a situation in which the sheet temperature increases form T_∞ in proportion to *r* and such that the amount of temperature increase along sheet increase with time.

The equations that governs the flow are:

$$\frac{\partial u}{\partial r} + \frac{u}{r} + \frac{\partial w}{\partial z} = 0, \tag{2.1}$$

$$\frac{\partial u}{\partial t} + u\frac{\partial u}{\partial r} + w\frac{\partial u}{\partial z} = \frac{\mu_{hnf}}{\rho_{hnf}}\frac{\partial^2 u}{\partial z^2}, \tag{2.2}$$

$$\frac{\partial T}{\partial t}+u\frac{\partial T}{\partial r}+w\frac{\partial T}{\partial z}=\frac{K_{hnf}}{\left(\rho C_P\right)_{hnf}}\frac{\partial^2 T}{\partial z^2}, \tag{2.3}$$

where $T(r,z,t)$ is the temperature and $w(r,z,t)$, and $u(r,z,t)$ are the components of the velocity toward z and r axes. μ_{hnf}, ρ_{hnf}, $\left(\rho C_p\right)_{hnf}$, and k_{hnf} denote the dynamic viscosity, density, heat capacity, and thermal conductivity of the hybrid nanofluids.

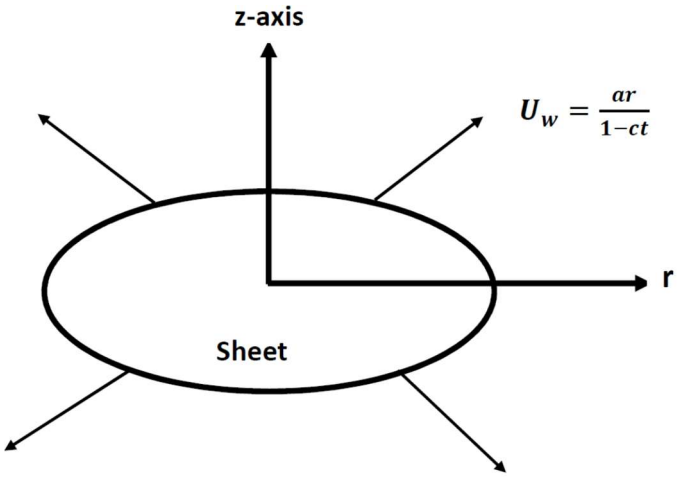

Fig.1. Geometry and coordinate system

In accordance with Devi [10-11], Abu-Nada and Oztop [21], fluid and hybrid nanofluid thermophysical properties are assessed using the equation demonstrated in Tab.1. Table 2 gives the same information as Oztop and Abu-Nada [21] regarding the base fluid and nanoparticles. In this case the subscripts $n1$, $n2$, f, and hnf stand for the Al_2O_3, Cu nanoparticles solid components, fluid and hybrid nanofluid.

Table 1. Thermophysical characteristics of hybrid nanofluid and fluid.

Property	Fluid	Hybrid nanofluid [10, 11]
Heat capacity	$\left(\rho C_p\right)_f$	$\left(\rho C_p\right)_{hnf}=\left(1-\phi_2\right)\left[\left(1-\phi_1\right)\left(\rho C_p\right)_f+\phi_1\left(\rho C_p\right)_{n1}\right]+\phi_2\left(\rho C_p\right)_{n2}$
Dynamic viscosity	μ_f	$\mu_{hnf}=\left\{\frac{\mu_f}{\left[\left(1-\phi_1\right)\left(1-\phi_2\right)\right]^{2.5}}\right\}$
Density	ρ_f	$\rho_{hnf}=\phi_2\rho_{n2}+\left(-\phi_2\right)\left[\left(1-\phi_1\right)\rho_f+\phi_1\rho_{n1}\right]$
Thermal conductivity	k_f	where $\frac{k_{hnf}}{k_{nf}}=\left[\frac{k_{n2}-2\phi_2\left(k_{nf}-k_{n2}+2k_{nf}\right)}{k_{n2}+\phi_2\left(k_{nf}-k_{n2}\right)+2k_{nf}}\right]$, $\frac{k_{nf}}{k_f}=\left[\frac{k_{n1}-2\phi_1\left(k_f-k_{n1}\right)+2k_f}{k_{n1}+\phi_1\left(k_f-k_{n1}\right)+2k_f}\right]$

Table 2. Fluid thermophysical characteristics and nanoparticles [21].

Characteristics	Cu	Al_2O_3	Water
$k(W/mK)$	*400*	*40*	*0.613*
$C_p(J/kgK)$	*385*	*765*	*4179*
$\rho(kg/m^3)$	*8933*	*3970*	*997.1*

The boundary conditions on the surface are that the velocity on the sheet is the stretching velocity of the sheet i.e. U_w, there is suction/injection through the sheet with velocity W_0 and the temperature of the sheet is maintained at T_w. Far away from the sheet there is no flow, and the temperature is T_∞. These conditions are provided by

$$u = U_w = \frac{ar}{1-ct}, \quad w = W_0, \quad T_w = T_\infty + \frac{br}{1-ct} \quad \text{at} \quad z = 0,$$
$$u \to 0, \quad T \to T_\infty \quad \text{as} \quad z \to \infty. \tag{2.4}$$

The similarity transformations for the present problem are given by

$$\eta = \frac{z}{r} Re^{1/2}, \quad \psi(r,z) = -r^2 U_w Re^{-1/2} f(\eta), \quad \theta = \frac{T - T_\infty}{T_w - T_\infty}. \tag{2.5}$$

Here $\psi(r,z)$ represents the function of stream provided by $u = -\frac{1\partial\psi}{r\partial z}$, $w = \frac{1\partial\psi}{r\partial r}$ and $Re = \frac{rU_w}{\nu}$ represent the local Reynolds number.

Substituting Eq.(2.5) into Eqs (2.1-2.3), results in the following non-dimensional equations.

$$\left[\frac{\mu_{hnf}\rho_f}{\rho_{hnf}\mu_f}\right] f''' + 2ff'' - f'^2 - A\left[f' + \frac{1}{2}\eta f''\right] = 0, \tag{2.6}$$

$$\left[\frac{1}{Pr}\frac{K_{hnf}(\rho C_p)_f}{(\rho C_p)_{hnf} K_f}\right]\theta'' + 2f\theta' - f'\theta - A\left[\theta + \frac{1}{2}\eta\theta'\right] = 0 \tag{2.7}$$

where $A = \frac{c}{a}$ represent the parameter of unsteadiness, $Pr = \frac{\nu}{\alpha_f}$ represent the Prandtl number.

The accompanying boundary are changed to the subsequent form

$$\theta(\eta) = 1, \quad f(\eta) = S, \quad \frac{df(\eta)}{d\eta} = 1 \quad \text{at} \quad \eta = 0,$$
$$\theta(\eta) \to 0, \quad \frac{df(\eta)}{d\eta} \to 0 \quad \text{as} \quad \eta \to \infty. \tag{2.8}$$

S is the suction/injection parameter given by $W_0 = -2S\left[\frac{U_w \nu}{r}\right]^{1/2}$. $S > 0$ signifies suction and $S < 0$ signifies injection.

The heat transfer rate (Nusselt number Nu) and coefficient of skin friction C_f are defined by:

$$N_u = -\frac{r}{(T_w - T_\infty)}\left(\frac{\partial T}{\partial z}\right)_{z=0}, \quad C_f = \frac{2}{\rho U_w^2}\mu\left(\frac{\partial u}{\partial z}\right)_{z=0}. \tag{2.9}$$

The non-dimensional form of Nusselt number Nu and skin friction coefficient C_f are:

$$Re^{-1/2} Nu = -\theta'(0), \frac{1}{2} Re^{1/2} C_f = f''(0). \tag{2.10}$$

2.2. Method of solution

The basic principal of the Successive Linearization Method (SLM) is the assumption that the functions $\theta(\eta)$ and $f(\eta)$ can be taken as

$$\theta(\eta) = \theta_j(\eta) + \sum_{k=0}^{j-1}\theta_k(\eta), f(\eta) = f_j(\eta) + \sum_{k=0}^{j-1} f_k(\eta). \tag{2.11}$$

Here, f_j and θ_j $(j = 1,2,3,...)$ are unknown functions and f_k and θ_k, $(k \geq 1)$ are the approximations that can be acquired repeatedly by computing the solution of linear portion of the equations that arises by putting Eq.(2.11) into Eqs (2.6) and (2.7). The basic principle concerning the SLM is that when j grows in size, f_j and θ_j becomes progressively smaller and thus ignored, i.e.,

$$\lim_{j\to\infty} f_j = \lim_{j\to\infty} \theta_j = 0. \tag{2.12}$$

The initial assumptions for $f_0(\eta)$ and $\theta_0(\eta)$ are made in order to meet the boundary conditions. The differential equations for f_j and θ_j, $(j \geq 1)$ are found by substituting Eq.(2.11) in Eqs (2.6) and (2.7), and then taking only the linear terms.

$$a_1 f_j''' + a_2 f_j'' + a_3 f_j' + a_4 f_j = r_1, \tag{2.13}$$

$$b_1 f_j' + b_2 f_j + b_3 \theta_j'' + b_4 \theta_j' + b_5 \theta_j = r_2. \tag{2.14}$$

The linearized boundary conditions are

$$f_j(0) = f_j'(0) = f_j'(\infty) = 0, \quad \theta_j(0) = \theta_j(\infty) = 0, \tag{2.15}$$

where the coefficients a_k, $(k = 1,2,3,4)$, b_m, $(m = 1,2,3,4,5)$, and r_p $(p = 1,2)$ are:

$$a_1 = \frac{\mu_{hnf}/\mu_f}{\rho_{hnf}/\rho_f}, \quad a_2 = 2\sum_{k=0}^{j-1} f_k - \frac{A}{2}\eta, \quad a_3 = -\left[2\sum_{k=0}^{j-1} f_k' + A\right], \quad a_4 = 2\sum_{k=0}^{j-1} f_k',$$

$$r_1 = -a_1\sum_{k=0}^{j-1} f_k''' + \left[-2\sum_{k=0}^{j-1} f_k + \frac{A\eta}{2}\right]\sum_{k=0}^{j-1} f_k'' + \left(\sum_{k=0}^{j-1} f_k'\right)^2 + A\sum_{k=0}^{j-1} f_k', \quad b_1 = -\sum_{k=0}^{j-1}\theta_k,$$

$$b_2 = 2\sum_{k=0}^{j-1}\theta_k', \quad b_3 = \frac{1}{Pr}\frac{K_{hnf}/K_f}{\left(\rho C_p\right)_{hnf}/\left(\rho C_p\right)_f}, \quad b_4 = 2\sum_{k=0}^{j-1} f_k - \frac{A}{2}\eta, \quad b_5 = -\left[A + \sum_{k=0}^{j-1} f_k'\right],$$

$$r_2 = -b_3\sum_{k=0}^{j-1}\theta_k'' + \left[\frac{A}{2}\eta - 2\sum_{k=0}^{j-1} f_k\right]\sum_{k=0}^{j-1}\theta_k' + \left(A + \sum_{k=0}^{j-1} f_k'\right)\sum_{k=0}^{j-1}\theta_k.$$

After calculating each solution for f_j and θ_j, $(j \geq 1)$ by repeatedly solving Eqs (2.13-2.14), the approximate values for $\theta(\eta)$ and $f(\eta)$ are obtained as follows.

$$\theta(\eta) \approx \sum_{p=0}^{P}\theta_p(\eta), f(\eta) \approx \sum_{p=0}^{P} f_p(\eta) \tag{2.16}$$

where *p* denotes the SLM approximation order.

The system of Eqs (2.13-2.14) may be solved analytically (if possible) or numerically using any methods, most notably collocation methods, finite differences, shooting technique based on Runge-Kutta, and finite elements. This study uses the spectral collocation method using Chebyshev polynomials. The method requires a few grid points to give very accurate results and take less computation time. This method is used mainly because it offers the simplest treatment of derivatives and all types of boundary conditions. This technique is based on using the Chebyshev interpolating polynomials to approximate the unknown functions in a way that allows them to collocate at the Gauss-Lobatto points,

$$\xi_i = \cos\frac{\pi i}{M}, \quad i = 0, 1, ..., M \tag{2.17}$$

where $M+1$ collocation points are utilized.

To put the method into practice, the domain truncation technique is used to change the physical domain into the domain $[0, L]$. The domain again changed to $[-1, 1]$ the using

$$\frac{\eta}{L} = \frac{\xi + 1}{2}, -1 \leq \xi \leq 1 \tag{2.18}$$

where L represents the scaling value that activates the boundary condition at infinity.

At the collocation positions the undefined functions f_j and θ_j are approximated by the Chebyshev interpolating polynomials

$$f_j(\xi) \approx \sum_{p=0}^{M} f_j(\xi_p) T_p(\xi_i), \quad \theta_j(\xi) \approx \sum_{p=0}^{M} \theta_j(\xi_p) T_p(\xi_i) \tag{2.19}$$

where $i = 0,1,2,....,M$ and T_p stands for p^{th} Chebyshev polynomial described as

$$T_p(\xi) = \cos\left[p \cos^{-1}(\xi) \right].$$

The unknown function derivatives are computed as

$$\frac{d^a f_j}{d\eta^a} = \sum_{p=0}^{M} D_{pi}^a \quad f_j(\xi_p), \quad \frac{d^a \theta_j}{d\eta^a} = \sum_{p=0}^{M} D_{pi}^a \theta_j(\xi_p), \quad i = 0,1,2,...,M . \tag{2.20}$$

Here $D = \frac{2}{L} D$, where D stands for Chebyshev spectral differentiation matrix, and a is the order of differentiation. The matrix equation that results from substituting Eqs (2.18-2.20) in Eqs (2.13-2.15) is as follows.

$$B_{j-1} X_j = Q_{j-1} \tag{2.21}$$

along with the conditions on the boundary

$$f_j(\xi_M) = \sum_{p=0}^{M} D_{0p} f_j(\xi_p) = \sum_{p=0}^{M} D_{Mp} f_j(\xi_p) = \theta_j(\xi_M) = \theta_j(\xi_0) = 0 \tag{2.22}$$

in which B_{j-1} is a square matrix of order $2(M+1)$ and X_j, R_{j-1} are column vectors of order $(2M+1)\times 1$ described by

$$B_{j-1} = \begin{bmatrix} B_{11} & B_{12} \\ B_{21} & B_{22} \end{bmatrix}, \quad X_j = \begin{bmatrix} F_j \\ \Theta_j \end{bmatrix}, \quad Q_{j-1} = \begin{bmatrix} q_1 \\ q_2 \end{bmatrix}, \tag{2.23}$$

where

$$B_{11} = a_1 D^3 + a_{12} D^2 + a_3 D + a_3, \quad B_{12} = 0, \quad B_{21} = b_1 D + b_2, \quad B_{22} = c_3 D^2 + b_4 D + b_5,$$

$$F_j = [f_j(\xi_0), f_j(\xi_1), ..., f_j(\xi_{(M-1)}), f_j(\xi_M)]^T, \quad \Theta_j = \left[\theta_j(\xi_0), \theta_j(\xi_1), ..., \theta_j(\xi_{M-1}), \theta_j(\xi_M)\right]^T,$$

$$q_1 = \left[r_1(\xi_0), r_1(\xi_1), ..., r_1(\xi_{M-1}), r_1(\xi_M)\right]^T, \qquad q_2 = \left[r_2(\xi_0), r_2(\xi_1), ..., r_2(\xi_{M-1}), r_2(\xi_M)\right]^T,$$

a_p $(p = 1,2,3)$ and b_l, $(l = 1,2,3,4)$, defined above are diagonal matrices of order ($M+1$), and the transpose is indicated by the superscript T. On Eq.(2.21), the boundary constraints (2.22) are applied through altering the first and last rows of B and r_p.

3. Results and discussion

In the current investigation, for distinct values of the solid volume fraction of ϕ_1 for Al_2O_3, ϕ_2 for Cu, suction/injection parameter S, and unsteadiness parameter A, the Nusselt number Nu, coefficient of skin friction C_f, velocity, and temperature are determined and are graphically represented. Unless otherwise stated, the numerical computations are performed using $\phi_1 = 0.1$, $\phi_2 = 0.1$, $A = 0.5$, and $S = 0.5$ to assess the influence of all of the parameters involved. Eqs (2.16-2.17) are linearized using the successive linearization procedure, and then the solving system is solved using the collocation method. The resultant Nusselt number and skin friction coefficient are compared with the findings of earlier studies for $\phi_1 = \phi_2 = 0$. A well-justified comparison between our results and those for $f''(0)$ and $\theta'(0)$ is presented in Tab.3.

Table 3. Comparison between $\theta'(0)$ and $f''(0)$ values at the surface by the current strategy with Shahzad *et al.* [6] finding.

A	S	Pr	$f''(0)$		$\theta'(0)$	
			current values	Shahzad *et al*. [6]	current values	Shahzad *et al*. [6]
0.5	*1*	*1*	*–2.6559727*	*–2.655999*	*–2.6559727*	*–2.655999*
0.5	*0.5*	*1*	*–1.9078958*	*–1.907999*	*–1.9078958*	*–1.907999*
0.5	*0*	*1*	*–1.3089787*	*–1.308999*	*–1.3089787*	*–1.308999*
0.5	*–0.5*	*1*	*–0.8872083*	*–0.887200*	*–0.8872083*	*–0.887200*
0.5	*–1*	*1*	*–0.6204663*	*–0.620400*	*–0.6204663*	*–0.620400*
0	*0.5*	*1*	*–1.7989331*	*–1.798999*	*–1.7996845*	*–1.798999*
0.5	*0.5*	*0.5*	*–1.9077295*	*–1.907999*	*–1.1196124*	*–1.119999*
0.5	*0.5*	*0.7*	*–1.9077295*	*–1.907999*	*–1.4502730*	*–1.450000*
1	*0.5*	*1*	*–2.0169687*	*–2.016999*	*–2.0168719*	*–2.016999*

To check the convergence, the code written to solve Eqs (2.13) to (2.14) along with the boundary conditions (2.15) using the pseudo-spectral method is executed for the skin friction coefficient and heat transfer rate by changing the number of collocation points N as $N = 40, 60, 80, 100$ and 120, and in each case we found very excellent agreement between them, which can be observed from Tab.4.The same tendency is witnessed by changing the values of parameters. Hence, a grid size of *100* is adopted to be satisfactory for the convergence criterion of 10^{-4}.

To validate the accuracy of the method, the code developed is verified by comparing the present numerical results of the skin friction coefficient with the published results of Khan and Shahzad [6], and the computed results are presented in Tab.5. It is evident from Tab.5 that the present results are in good agreement with the results of Khan and Shahzad [6].

Table 4. Convergence of $f''(0)$ and $-\theta'(0)$ by SLM.

Number of grid points	$f''(0)$	$-\theta'(0)$
40	*–2.2064352*	*–1.1726257*
60	*–2.2016276*	*–1.1700795*
80	*–2.1909501*	*–1.1698968*
100	*–2.1907222*	*–1.1695897*
120	*–2.1907162*	*–1.1695689*

Table 5. Comparative analysis for the values of skin friction coefficient $f''(0)$ by the present method for $P_r = 1,\ \ \phi_1 = 0,\ \ \phi_2 = 0$, with the results of Khan and Shahzad [6].

Present results	Khan and Shahzad [6]
−1.907968	*−1.907999*

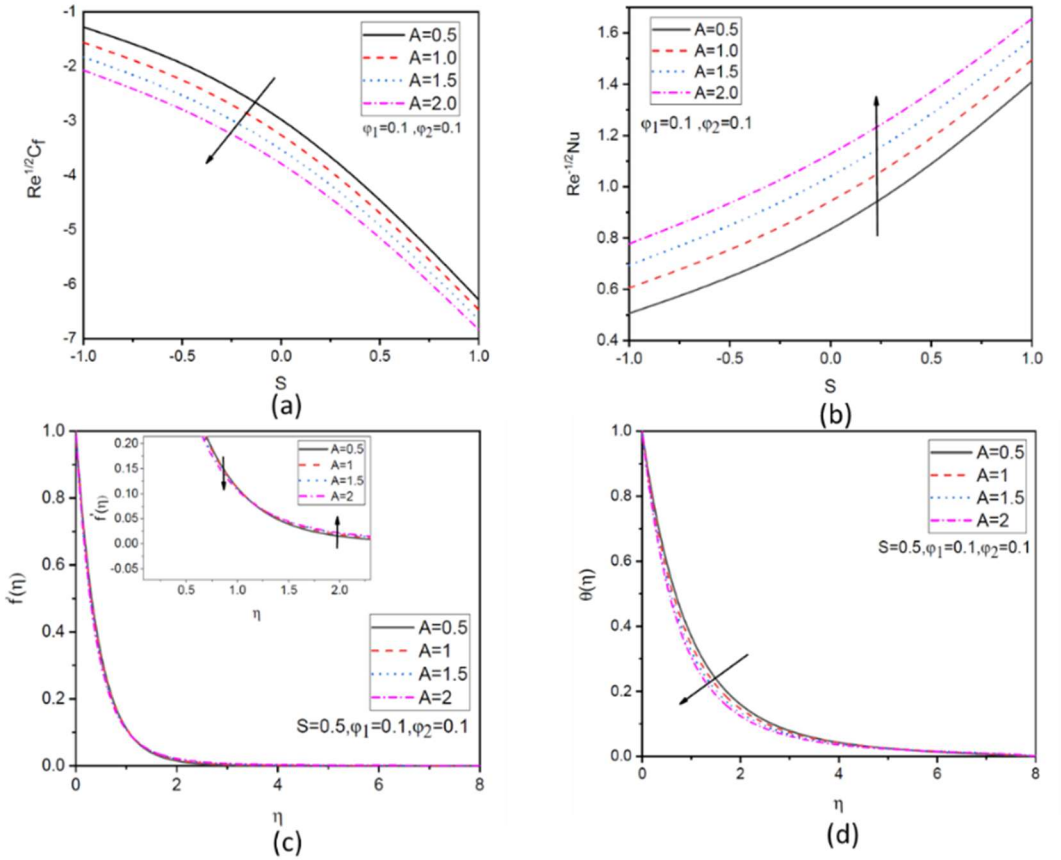

Fig.2. Variation of (a) skin friction coefficient, (b) Nusselt number, (c) velocity and (d) temperature with unsteadiness parameter A.

Figure 2 demonstrates the impact of the parameter of unsteadiness A over the temperature, velocity, heat transfer rate, and skin friction coefficient $f''(0)$. An enhancement in A decreases the skin friction $f''(0)$, as demonstrated in Fig.2(a). This is due to the development of the velocity boundary layer is caused solely on the stretching plate Fig.2(b) demonstrates that $-\theta'(0)$ enhances as the value of parameter A increases. Physically, it means that the temperature gradient at the surface increases as A increases, which imply the increase of heat transfer rate at the surface. The rise in parameter A led to an initial decrease in velocity but later a slowly increment in the velocity as depicted in Fig.2(c). It is noticed from Fig.2(d) that an enhancement in the parameter A led to the decrease in temperature. Physically, the dependency of hybrid nanofluid flow for the rising values of the unsteadiness parameter shows that the rate of cooling effects is much more for the transient currents and as a result, it produces less heat and consequently, the chunkiness of the thermal boundary layer and also the temperature distribution significantly diminishes.

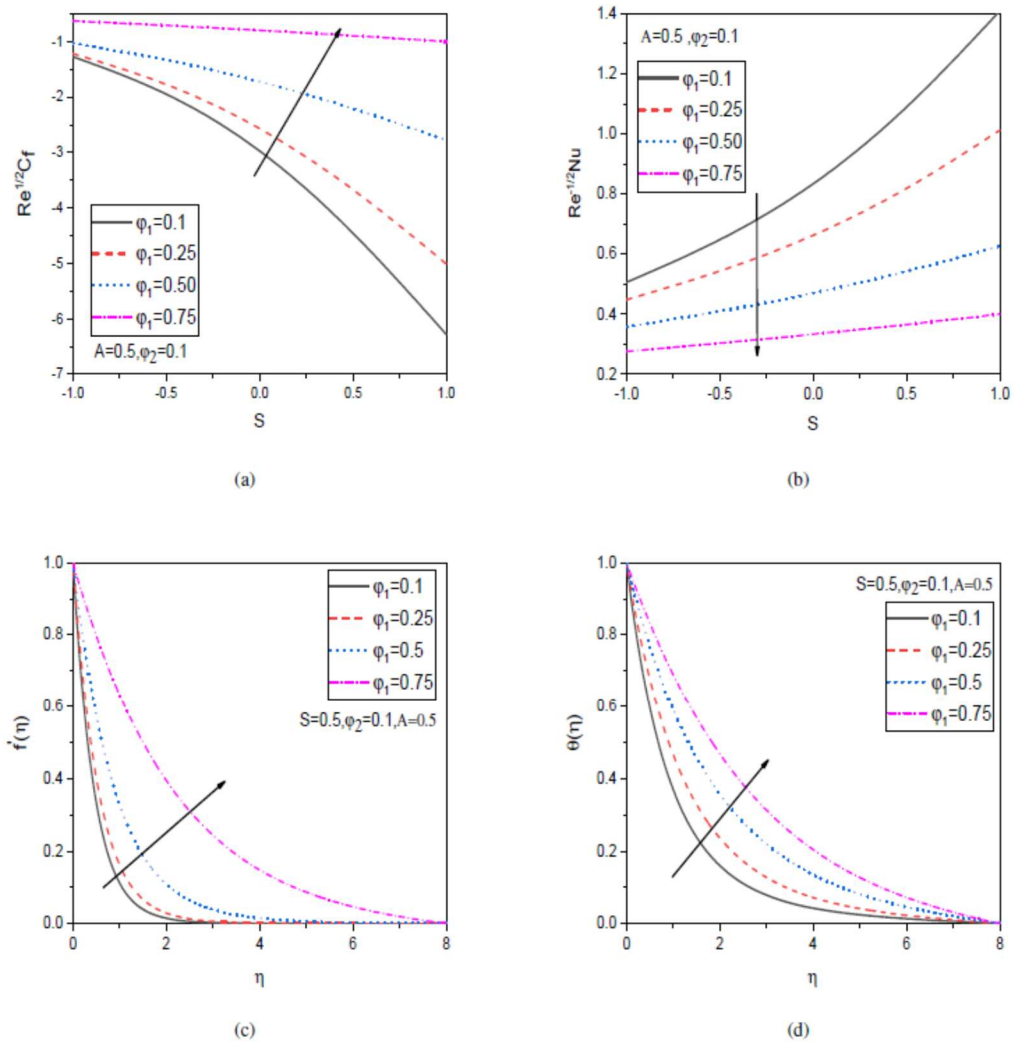

Fig.3. Variation of (a) skin friction coefficient, (b) Nusselt number, (c) velocity and (d) temperature with unsteadiness parameter ϕ_1.

The impact of ϕ_1 on heat transfer rate $-\theta'(0)$, coefficient of skin friction $f''(0)$, temperature, and velocity is described in Fig.3. It is observed that as ϕ_1 increases, skin friction $f''(0)$ escalates, as given in Fig.3(a), and $-\theta'(0)$ diminishes, as presented in Fig.3(b). It is noticed that the rise in parameter ϕ_1 enhances velocity as depicted in Fig.3(c) and also increases temperature as displayed in Fig.3(d). This occurs because nanoparticles enhance the thermal conductivity of the fluid, allowing more heat to be retained.

The influence of ϕ_2 on heat transfer rate $-\theta'(0)$, coefficient of skin friction $f''(0)$, temperature, and velocity are depicted in Fig.4 .The skin friction $f''(0)$ decreases as the variable ϕ_2 rises, as illustrated in Fig.4(a), and $-\theta'(0)$ diminishes as ϕ_2 increases, as displayed in Fig.4(b). It is seen that the rise in parameter ϕ_2 diminishes velocity as shown in Fig.4(c), indicating that higher concentrations of nanoparticles may hinder fluid motion. As the nanoparticle volume fraction increases, the fluid's viscosity tends to rise due to the higher concentration of solid particles, which can lead to a more substantial resistance to flow. In Fig.4(d), as the nanoparticle volume fraction () increases, the temperature rises. This occurs because nanoparticles enhance the thermal conductivity of the fluid, allowing more heat to be retained. In general, the nanoparticles dissipate

some energy in the form of heat. At the same time, owing to the yield of two or more different nanoparticles may exert more dissipation of energy like heat which improves the thermal conductivity and the temperature distribution for the hybrid nanofluid. Hence, owing to the influence of two different nanoparticles as a result the thermal boundary layer thickness is also become increasing.

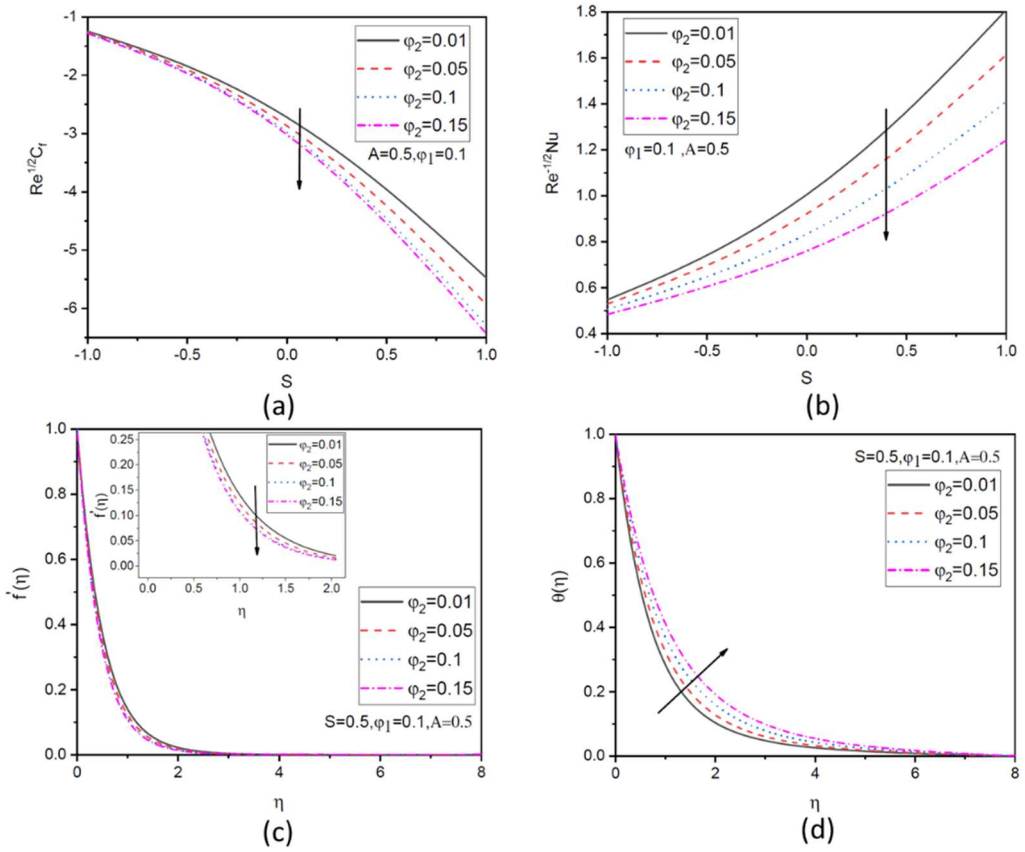

Fig.4. Variation of (a) Skin friction coefficient, (b) Nusselt number, (c) velocity and (d) temperature with unsteadiness parameter ϕ_2.

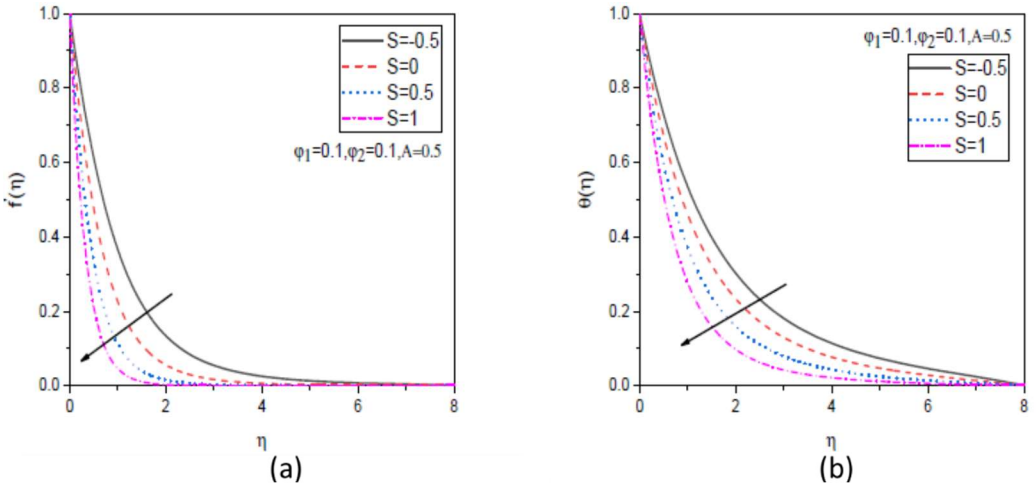

Fig.5. Variation of (a) velocity and (b) temperature with unsteadiness parameter *S*.

The outcome of the suction/injection variable S over temperature and velocity is demonstrated in Fig.5. Figure 5(a) illustrates that the velocity decreases as S enhances, and Fig.5(b) depicts that the temperature reduces as S enhances. In physical point of view, to see the response of the parameter S, the hybrid nanofluid is fetched closer to the wall surface of the sheet and consequently, it stops the vorticity dispersion.

4. Conclusion

In this paper, the nonlinear differential equations arising from the hybrid nanofluid past time-dependent sheet that is stretched radially under the impact of the unsteadiness parameter, suction or injection parameter, ϕ_1 and ϕ_2 at the surface are resolved by means of the SLM method. The effect of the parameters A, S, ϕ_1, and ϕ_2 over the pertinent physical quantities is scrutinized. The primary findings are outlined below.

– As the unsteadiness parameter and the volume fraction of copper nanoparticles increase, the skin friction decreases. Conversely, as the volume fraction of alumina nanoparticles increases, the skin friction also increases.
– A lower Nusselt number results from increasing the volume fractions of both copper and alumina nanoparticles, while a rise in unsteadiness contributes to a higher Nusselt number.
– As the volume fraction of alumina nanoparticles increases, the velocity increases, and as unsteadiness, suction/injection, and the volume of copper nanoparticles increase, the velocity decreases.
– The temperature increases with higher volume fractions of both copper and alumina nanoparticles, while it decreases with increasing values of the unsteadiness parameter and the suction/injection parameter.

The findings presented in this study open up intriguing possibilities for future research in the domain of different types of nanoparticles and Carbon nanotubes, nanoparticle size and shape, and flow in porous media. As this study does not include nanoparticle agglomeration and Brownian motion, it can be extended by including these effects. This research explores multi-physics and multi-scale modeling techniques to account for a broader range of phenomena, including chemical reactions or the heterogeneity of the porous medium, which could provide a more comprehensive understanding of the complex systems involving different nanoparticles.

Nomenclature

A – unsteadiness parameter,
$a,b,c(\geq 0)$ – constants.
C_f – coefficient of skin friction
C_p – specific heat at constant pressure
k_{hnf} – thermal conductivity of the hybrid nanofluid
Nu – heat transfer rate (Nusselt number)
Pr – Prandtl number
(r,z) – radial and axial coordinate axes
Re – local Reynolds number.
$T_\infty (T_w > T_\infty)$ – temperature of the surrounding medium
$T(r,z,t)$ – temperature
T_w – temperature at the stretched surface
$u(r,z,t)$, $w(r,z,t)$ – velocity components r and z direction
U_w – time-dependent stretching velocity

W_0 – suction/injection velocity

α – thermal diffusivity

μ – dynamic viscosity

ν – kinematic viscosity

$\psi(r,z)$ – stream function

ρ – density

Subscripts

f – for the fluid

hnf – for hybrid nanofluid

$n1$ – for the Al_2O_3 nanoparticles

$n2$ – for the Cu nanoparticles solid components

References

[1] Khan M., Mehwish M. and Rahman M.U. (2017): *On axisymmetric flow and heat transfer of Cross fluid over a radially stretching sheet*.– Results in Physics, vol.7, pp.3767-3772, https://doi.org/10.1016/j.rinp.2017.09.043.

[2] Ahmed J., Shahzad A., Begum A., Ali R. and Siddiqui N. (2017): *Effects of inclined Lorentz forces on boundary layer flow of Sisko fluid over a radially stretching sheet with radiative heat transfer*.– Journal of the Brazilian Society of Mechanical Sciences and Engineering, vol.39, No.8, pp.3039-3050, https://doi.org/10.1007/s40430-017-0744-y.

[3] Sreelakshmi K., Sarojamma G. and Murthy J.V. (2018): *Homotopy analysis of an unsteady flow heat transfer of a Jeffrey nanofluid over a radially stretching convective surface*.– Journal of Nanofluids, vol.7, No.1, pp.62-71, https://doi.org/10.1166/jon.2018.1425.

[4] Khan S.A., Yufeng N. and Ali B. (2019): *Multiple slip effects on magnetohydrodynamic axisymmetric buoyant nanofluid flow above a stretching sheet with radiation and chemical reaction*.– Symmetry, vol.11, No.9, pp.1171, https://doi.org/10.3390/sym11091171.

[5] Nayak B., Mishra S.R. and Krishna G.G. (2019): *Chemical reaction effect of an axisymmetric flow over radially stretched sheet*.– Propulsion and Power Research, vol.8, No.1, pp.79-84, https://doi.org/10.1016/j.jppr.2019.01.008.

[6] Shahzad A., Ali R., Hussain M. and Kamran M. (2017): *Unsteady axisymmetric flow and heat transfer over time-dependent radially stretching sheet*.– Alexandria Engineering Journal, vol.56, No.1, pp.35-41, https://doi.org/10.1016/j.aej.2016.08.030.

[7] Shahzad A., Gulistan U., Ali R., Iqbal A., Benim A.C., Kamran M., Khan S.U., Khan S.U. and Farooq A. (2020): *Numerical study of axisymmetric flow and heat transfer in a liquid film over an unsteady radially stretching surface*.– Mathematical Problems in Engineering, vol.2020, pp.1-9, https://doi.org/10.1155/2020/4346859.

[8] Srinivasacharya D. and Shravan Kumar R. (2022): *Artificial neural network modeling of the Casson fluid flow over unsteady radially stretching sheet with Soret and Dufour effects*.– Journal of Thermal Analysis and Calorimetry, vol.147, No.24, pp.14891-14903, https://doi.org/10.1007/s10973-022-11603-5.

[9] Choi S.U. and Eastman J.A. (1995): *Enhancing Thermal Conductivity of Fluids with Nanoparticles*.– Argonne National Lab (ANL), Argonne, IL (United States), No.ANL/MSD/CP-84938, https://www.osti.gov/biblio/196525.

[10] Anjali Devi S.P. and Uma Devi S.S. (2016): *Numerical investigation of hydromagnetic hybrid Cu-Al2O3/water nanofluid flow over a permeable stretching sheet with suction*.– International Journal of Nonlinear Sciences and Numerical Simulation, vol.17, No.5, pp.249-257, https://doi.org/10.1515/ijnsns-2016-0037.

[11] Uma Devi S.S. and Anjali Devi S.P. (2017): *Heat transfer enhancement of Cu-Al2O3/water hybrid nanofluid flow over a stretching sheet*.– Journal of the Nigerian Mathematical Society, vol.36, No.2, pp.419-433, https://doi.org/10.1016/j.jnnms.2017.06.001.

[12] Hayat T. and Nadeem S. (2017): *Heat transfer enhancement with Ag-CuO/water hybrid nanofluid*.– Results in Physics, vol.7, pp.2317-2324, https://doi.org/10.1016/j.rinp.2017.06.034.

[13] Yousefi M., Dinarvand S., Yazdi M.E. and Pop I. (2018): *Stagnation-point flow of an aqueous titania-copper hybrid nanofluid toward a wavy cylinder*.– International Journal of Numerical Methods for Heat and Fluid Flow, vol.28, No.7, pp.1716-1735, https://doi.org/10.1108/HFF-01-2018-0009.

[14] Subhani M. and Nadeem S. (2019): *Numerical analysis of micropolar hybrid nanofluid*.– Applied Nanoscience, vol.9, No.4, pp.447-459, https://doi.org/10.1007/s13204-018-0925-1.

[15] Ghadikolaei S.S., Yassari M., Sadeghi H., Hosseinzadeh K. and Ganji D.D. (2017): *Investigation on thermophysical properties of TiO2-Cu/H2O hybrid nanofluid transport dependent on shape factor in MHD stagnation point flow*.– Powder Technology, vol.322, pp.428-438, https://doi.org/10.1016/j.powtec.2017.09.006.

[16] Usman M., Hamid M., Zubair T., Haq R.U. and Wang W. (2018): *Cu-Al2O3/water hybrid nanofluid through a permeable surface in the presence of nonlinear radiation and variable thermal conductivity via LSM*.– International Journal of Heat and Mass Transfer, vol.126, pp.1347-1356, https://doi.org/10.1016/j.ijheatmasstransfer.2018.06.005.

[17] Rostami M.N., Dinarvand S. and Pop I. (2018): *Dual solutions for mixed convective stagnation-point flow of an aqueous silica-alumina hybrid nanofluid*.– Chinese Journal of Physics, vol.56, No.5, pp.2465-2478, https://doi.org/10.1016/j.cjph.2018.06.013.

[18] Waini I., Ishak A. and Pop I. (2019): *Unsteady flow and heat transfer past a stretching/shrinking sheet in a hybrid nanofluid*.– International Journal of Heat and Mass Transfer, vol.136, pp.288-297, https://doi.org/10.1016/j.ijheatmasstransfer.2019.02.103.

[19] Waini I., Ishak A. and Pop I. (2019): *Hybrid nanofluid flow and heat transfer past a permeable stretching/shrinking surface with a convective boundary condition*.– Journal of Physics: Conference Series, vol.1366, No.1, pp.012022, https://doi.org/10.1088/1742-6596/1366/1/012022.

[20] Tiwari R.K. and Das M.K. (2007): *Heat transfer augmentation in a two-sided lid-driven differentially heated square cavity utilizing nanofluids*.– International Journal of Heat and Mass Transfer, vol.50, No.9-10, pp.2002-2018, https://doi.org/10.1016/j.ijheatmasstransfer.2006.09.004.

[21] Oztop H.F. and Abu-Nada E. (2008): *Numerical study of natural convection in partially heated rectangular enclosures filled with nanofluids*.– International Journal of Heat and Fluid Flow, vol.29, No.5, pp.1326-1336, https://doi.org/10.1016/j.ijheatfluidflow.2008.04.009.

[22] Das K. (2023): *Computational analysis on magneto hybrid nanofluid flow with water as base fluid and nanoparticles as aluminium oxide (Al2O3) and copper (Cu) induced by a convectively heated stretching sheet in presence of surface slip*.– Waves in Random and Complex Media, pp.1-15, https://doi.org/10.1080/17455030.2023.2172082.

[23] Ali S., Shaiq S., Shahzad A., Sohail M. and Naseem T. (2024): *Numerical thermal investigation of radiative magnetohydrodynamics axisymmetric Cu-Al2O3/H2O hybrid nanofluid flow over an unsteady radially stretched surface*.– International Journal of Ambient Energy, vol.45, No.1, pp.2321210, https://doi.org/10.1080/01430750.2024.2321210.

[24] Abbas T., Khalil S. and Sattar F.A. (2025): *Impact of variable fluid properties and viscous dissipation on hybrid nanofluid (Cu–Al2O3/H2O) flow past a porous stretching sheet*.– Multiscale and Multidisciplinary Modeling, Experiments and Design, vol.8, No.7, pp.333, https://doi.org/10.1007/s41939-024-00456-x.

Received: September 6, 2025

Revised: February 24, 2026